Proceedings of the 15th International Heat Transfer Conference, IHTC-15
August 10-15, 2014, Kyoto, Japan

IHTC15-9168

NUMERICAL TOPOLOGY OPTIMIZATION OF HEAT SINKS

Tijs Van Oevelen* **& Martine Baelmans**

KU Leuven, Department of Mechanical Engineering, Celestijnenlaan 300A, 3001, Leuven, Belgium

ABSTRACT

The availability of flexible production techniques challenges their full exploitation during thermo-hydraulic design of micro heat sinks. In this context, a systematic approach capable to take advantage of the practically unlimited design freedom is highly desirable. Therefore, we propose to use topology optimization, a numerical design optimization method well-established in structural mechanics problems. In this paper, the fundamentals of topology optimization, and its application in thermo-hydraulic problems specifically, are pointed out. The method is applied to a practical heat sink model and the necessary adjoint gradient calculation framework is developed. Our results show that topology optimization can come up with innovative design concepts for maximizing the heat transfer of a constant temperature heat source.

KEY WORDS: Computational methods, Optimal control, Topology optimization, Heat transfer enhancement, Thermal management, Thermal design, Heat exchanger, Heat sink, MEMS, Electronic equipment cooling

1. INTRODUCTION

The development of liquid cooling for microelectronics components has made a big leap due to the work by Tuckerman & Pease in the early eighties [36]. They demonstrated that by scaling down the dimensions of the heat transfer surfaces in the heat sink, power densities above $1000\frac{\mathrm{W}}{\mathrm{cm}^2}$ are feasible. Their result is attributed to the increase in heat transfer coefficients and heat transfer surface area density.

The microchannel heat transfer technology has since then witnessed further improvements. These have been made either by optimizing the heat sink dimensions, and by changes to the structural concept of the heat sink. Several alternatives for the microchannel layout have been proposed, including changes to the overall layout of the flow network, as well as local heat transfer enhancement features.

A lot of work on optimizing heat sink dimensions (channel width, fin width…) has been performed with analytic models. Typically, the thermal resistance of the heat sink R_{hs} is minimized, for a fixed pressure drop (a.o. Knight et al [18, 19], Yin & Bau [42], Bau [3], Wei & Joshi [38], Kim [17], Liu & Garimella [25] and Stevens et al [33]):

$$R_{\mathrm{hs}} = \frac{T_{\mathrm{s}} - T_{\mathrm{i}}}{\dot{Q}} = \frac{\Delta T}{\dot{Q}} \tag{1}$$

where T_{s} and T_{i} are respectively the heat source temperature and the coolant inlet temperature. $\dot{Q}$ is the total heat transfer. Limited by the accuracy of the models used, improved modeling has been a continuous goal in this research area. This is evidenced by the vast amount of work that can be found on better correlations for heat

*Corresponding Tijs Van Oevelen: tijs.vanoevelen@mech.kuleuven.be; phone: +32 16 322511; fax: +32 16 322985

transfer and fluid flow. Also, numerical models have been used for evaluating the performance of micro heat sink designs. Such work has been performed by Weisberg et al [40], Yin & Bau [42], Fisher & Torrance [12], Ruy et al [29, 30], Kim [17], Li & Peterson [22, 23], Husain & Kim [14, 15], Kou et al [20] and Chen et al [8].

Alternatives for the microchannel layout include heat sinks with multiple collectors to reduce the total length of the flow paths (Kandlikar & Upadhye [16] on the split-flow arrangement and Harpole & Eninger [13], Copeland [10] and Ryu et al [30] on manifold heat sinks). Heat transfer enhancement is also achieved by the use of fins instead of channels. These have a local improvement effect because of the boundary layer that is regularly rebuilt, leading to higher heat transfer coefficients. Examples are found in Bejan & Morega [5], Yin & Bau [41], Colgan et al [9] and Li et al [21]. Other design concepts are stacked microchannels [39], microjets [21, 34], (radially) branched channels [4, 28, 37] and perforated fins [31]. Hybrid concepts have also been investigated [2, 34].

Despite these innovations, a systematic approach to topological design of the flow network is missing. Furthermore, the availability of versatile MEMS (microelectromechanical systems) fabrication processes, such as deep reactive ion etching (DRIE), offers flexibility and thus opportunities for the design of heat sinks, which should be reflected in the design process. In this paper, we provide a means to meet these concerns by topology optimization, a numerical design optimization method. The philosophy of such methods is to approach the design by formulating and solving an optimization problem, i.e. finding the optimum of an objective function over a set of parameters subject to constraints. Topology optimization sticks out because of its peculiar parameterization, which allows boundaries to appear and vanish during the optimization process. A comprehensive introduction to the method is provided by Bendsøe & Sigmund [6].

The applications of topology optimization to problems involving fluid mechanics and/or heat transfer are limited. Early work in this field has been performed by Borrvall & Petersson [7] on Stokes flows. In their approach, the design is locally parameterized by the porosity of the flow. This is the local volume fraction of fluid with respect to the total volume. The porosity is allowed to range from 0 (pure solid) to 1 (pure fluid) and determines the permeability of the flow, which is included in the momentum equations by a Darcy-type loss term. Further work on convective heat transfer applications has been performed by Okkels et al [26], Andreasen et al [1] and Dede [11].

In this paper, we discuss the required steps for topology optimization of micro structured heat sinks. Section 2 is dedicated to the flow and heat transfer modeling of the heat sink. In Section 3, the design optimization problem is formulated. We define the objective function and constraints, and formalize the design parameterization. Our numerical solution approach is outlined in Section 4. This covers the adjoint gradient calculation framework, the numerical model implementation and the optimization algorithm. Next, the method is applied to a test case in Section 5, in which the thermal resistance of the heat sink is minimized. The results are discussed in terms of structural layout and performance. A sensitivity analysis of the most important parameters is included. Section 6 provides a general discussion and evaluation of the results, in relation to literature. Finally, a summary and our conclusions are given in Section 7.

2. HEAT SINK MODEL

We consider the problem of cooling a constant temperature heat source T_s. The micro heat sink is attached on top of the heat source as in Figure 1(a). Perfect heat transfer to the bottom side of the heat sink is assumed. Thus, the temperature there is also T_s. Heat is extracted from the source and removed via convective heat transfer. For this purpose, a liquid coolant is pumped through the heat sink. The temperature at the inlet of the flow is T_i, and the static pressure drop over the heat sink is Δp.

The heat sink is made from a silicon wafer by a high aspect-ratio etching technique such as DRIE. This means that possible designs are essentially two-dimensional if the etch depth H is uniform. Material is etched away according to the configuration provided by the mask in the photolithography step. The design domain is

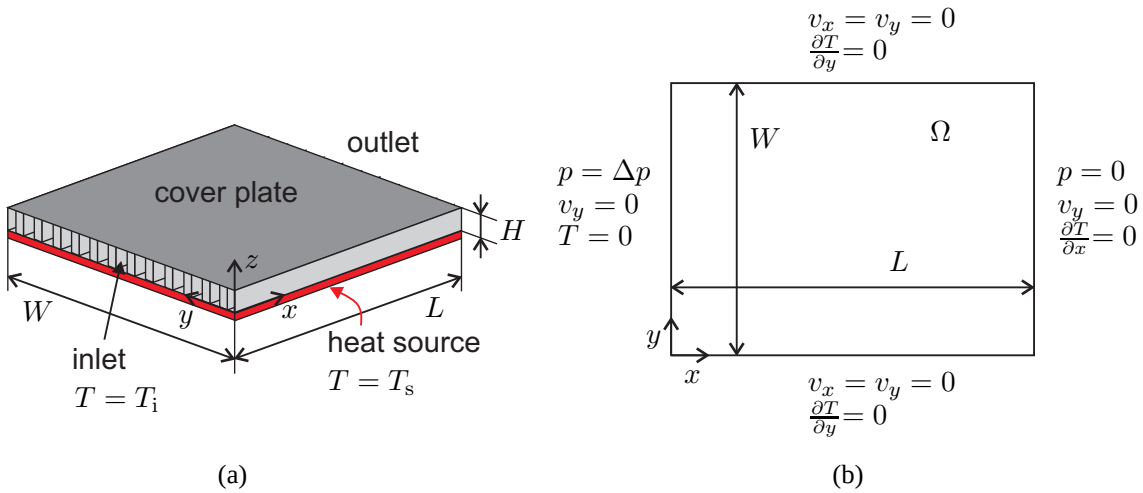

(a) (b)

Fig. 1 (a) Schematic layout of heat sink with constant temperature heat source, (b) Computational domain and boundary conditions

therefore a rectangular box $L \times W$, the surface area of the heat source, see Figure 1(b). Finally, a cover plate is attached on top of the heat sink to close the channels.

2.1 Mixed fluid-solid model equations

Following the approach of Borrvall & Petersson [7] for modeling the flow, a Darcy loss term is included in the momentum equations to model the effect of internal structures on the flow. The velocity $\mathbf{v}$ and pressure p fields are determined by the steady flow equations:

$$\nabla \cdot \mathbf{v} = 0 \tag{2}$$

$$\nabla \cdot (\rho \mathbf{v}\mathbf{v}) = -\nabla p + \nabla \cdot (\mu \nabla \mathbf{v}) - \frac{\mu}{\kappa}\mathbf{v} \tag{3}$$

where ρ and μ are respectively the mass density and the dynamic viscosity of the coolant, and κ is the permeability of the flow. The permeability depends locally on the design, i.e. κ is ∞ where the domain contains fluid and 0 in the solid material. As such, the model collapses to the steady, incompressible Navier-Stokes equations in the fluid and a zero-velocity condition in the solid.

The heat transfer in the heat sink is modeled by the steady energy equation:

$$\nabla \cdot (\rho c_p \mathbf{v} T) = \nabla \cdot (k \nabla T) \tag{4}$$

where c_p is the heat capacity of the coolant and k the heat conductivity. The heat conductivity is influenced by the design and equals k_f for the fluid and k_s for the solid material. The heat transfer model reduces to a pure heat conduction equation in the solid, because $\mathbf{v}$ is zero there.

2.2 Two-dimensional model

To keep the model manageable within the optimization context, the model is reduced to two dimensions. To this end, the model equations are averaged over the height of the domain. Thus a two-dimensional model is

obtained. This gives rise to following set of model equations:

$$\nabla \cdot \langle \mathbf{v} \rangle = 0 \tag{5}$$

$$\nabla \cdot (K_{\mathrm{c,m}} \rho \langle \mathbf{v} \rangle \langle \mathbf{v} \rangle) = -\nabla \langle p \rangle + \nabla \cdot (\mu \nabla \langle \mathbf{v} \rangle) - \underbrace{\mu \left(\frac{1}{\kappa} + \frac{K_{\mathrm{d,m}}}{H^2} \right)}_{=\alpha} \langle \mathbf{v} \rangle \tag{6}$$

$$\nabla \cdot (K_{\mathrm{c,e}} \rho c_p \langle \mathbf{v} \rangle \langle T \rangle) = \nabla \cdot (k \nabla \langle T \rangle) + k \frac{K_{\mathrm{d,e}}}{H^2} (T_{\mathrm{s}} - \langle T \rangle) \tag{7}$$

where $\langle \cdot \rangle$ is the averaging operation over the height of the domain. Several coefficients have occured in the model equations due to the integration of velocity, pressure and temperature. They are defined by following relations:

$$K_{\mathrm{c,m}} = \left\langle \zeta(z')^2 \right\rangle \qquad K_{\mathrm{c,e}} = \left\langle \zeta(z') \xi(z') \right\rangle \tag{8}$$

$$K_{\mathrm{d,m}} = -\left\langle \frac{\partial^2 \zeta(z')}{\partial z'^2} \right\rangle \qquad K_{\mathrm{d,e}} = -\left\langle \frac{\partial^2 \xi(z')}{\partial z'^2} \right\rangle \tag{9}$$

where $z' = \frac{z}{H}$ is the dimensionless z-coordinate, $\zeta(z')$ and $\xi(z')$ are respectively the velocity and temperature profiles, defined by:

$$\zeta(z') = \frac{v_x(z')}{\langle v_x \rangle} = \frac{v_x(z')}{\langle v_x \rangle} \qquad \xi(z') = \frac{T_{\mathrm{s}} - T(z')}{T_{\mathrm{s}} - \langle T \rangle} \tag{10}$$

$K_{\mathrm{c,m}}$ and $K_{\mathrm{c,e}}$ are convective flux corrections in respectively the momentum and energy equations. $K_{\mathrm{d,m}}$ and $K_{\mathrm{d,e}}$ model the diffusive fluxes of momentum and energy, i.e. viscous stress and heat conduction, in the z-direction.

A priori assumptions about the z-profiles have to be made. Here, we make use of the profiles for fully developed flow between flat plates with spacing H. This results in the following values for the coefficients: $K_{\mathrm{c,m}} = 1.2$, $K_{\mathrm{d,m}} = 12$, $K_{\mathrm{c,e}} = 1.057$ and $K_{\mathrm{d,e}} = 2.569$. Notice that these values are in agreement with data for $f\mathrm{Re}$ and Nu between parallel plates (Shah & London [32]). Indeed,

$$f\mathrm{Re} \equiv 2K_{\mathrm{d,m}} = 24 \qquad \mathrm{Nu} \equiv 2\frac{K_{\mathrm{d,e}}}{K_{\mathrm{c,e}}} = 4.861 \tag{11}$$

In the remainder of the text, the averaging notation $\langle \cdot \rangle$ will be omitted. The boundary conditions to the two-dimensional model are provided in Figure 1(b).

3. DESIGN OPTIMIZATION PROBLEM

The application of topology optimization for heat sink design focusses on structuring flow channels in a heat conducting solid. Throughout the optimization process, structures and channels can (dis)appear. Mathematically, this comes down to dividing the design domain Ω into two sets of points so that one set contains all the solid material and the other all the fluid material. These sets do not need to be connected. Such parameterization of the design is possible, but the resulting binary optimization problem is hard to solve. Therefore, we use the material distribution method to relax the parameterization. In this method, the design is represented by the porosity, which is the local volume fraction of fluid:

$$\varepsilon(\mathbf{x}) = \frac{\text{liquid volume}}{\text{total volume}} \text{ in a small neighbourhood around } \mathbf{x} \tag{12}$$

The porosity ε is a continuous variable ranging from 0 (solid) to 1 (fluid). This makes the design problem differentiable, which is more practical to solve.

The influence of the porosity on the heat sink model is represented by the design-dependent parameters $\alpha(\varepsilon)$ and $k(\varepsilon)$ in (6) and (7) respectively. Here, $\alpha(\varepsilon)$ is defined as:

$$\alpha = \mu \left(\frac{1}{\kappa(\varepsilon)} + \frac{K_{\mathrm{d,m}}}{H^2} \right) \tag{13}$$

We use the interpolation function by Borrvall & Petersson [7] to calculate α for intermediate values of ε:

$$\alpha(\varepsilon) = \alpha_{\max} + (\alpha_{\min} - \alpha_{\max})\, \varepsilon \frac{1+q}{\varepsilon + q} \tag{14}$$

In this interpolation function, $\alpha_{\max}$ is the value for $\varepsilon = 0$. In theory, $\alpha_{\max}$ should equal ∞. Therefore in practice, it is given a large numerical value. $\alpha_{\min}$ is the value for $\varepsilon = 1$, which is $\mu \frac{K_{\mathrm{d,m}}}{H^2}$. q is a parameter that controls the shape of the interpolation function. Higher q results in higher α for the intermediate values of ε. The parameter q is used to control the amount of intermediate porosities in the solution of the optimization. In [7] it is argued that the interpolation of α should be linear to achieve a perfect 0-1 solution. This corresponds to setting $q \to \infty$. However, to avoid getting stuck in local optima, a lower value $q = 0.1$ is advised.

A linear interpolation function is used for the heat conductivity k:

$$k(\varepsilon) = \varepsilon k_{\mathrm{f}} + (1 - \varepsilon) k_{\mathrm{s}} \tag{15}$$

With this formalization of the parameterization, we have all ingredients to state the design optimization problem. The design goal is to achieve maximal total heat transfer $\dot{Q}$ from the heat source to the heat sink. This is equivalent to the minimization of its thermal resistance. The total heat transfer $\dot{Q}$ is calculated as the integral of the source term in (7). The optimization problem is written as follows:

$$\begin{aligned} \max_{\varepsilon, \mathbf{v}, p, T} \quad & J(\varepsilon, \mathbf{v}, p, T) = \dot{Q} \equiv \int_{\Omega} k(\varepsilon) \frac{K_{\mathrm{d,e}}}{H^2} \left(T_{\mathrm{s}} - T\right) \mathrm{d}\mathbf{x} \\ & \text{subject to:} \\ & \qquad \text{model equations: (5), (6) and (7)} \\ & \qquad \text{boundary conditions: Fig. 1(b)} \\ & \qquad 0 \leq \varepsilon(\mathbf{x}) \leq 1 \end{aligned} \tag{16}$$

4. NUMERICAL APPROACH

4.1 Adjoint equations and gradient calculation

To solve the optimization problem (16), information about the effect of ε on the value of the cost functional is needed. We therefore need the gradient of the reduced cost functional:

$$\hat{J}(\varepsilon) = J(\varepsilon, \phi(\varepsilon)) \tag{17}$$

where $\phi(\varepsilon) = (\mathbf{v}, p, T)^{\mathrm{T}}$ is the solution of the model equations (5)–(7), in short written as $M(\varepsilon, \phi) = 0$. We apply the adjoint method, which is considered the state-of-the-art method in PDE optimization problems. Therefore, we define following Lagrangian functional:

$$L(\varepsilon, \phi, \phi^*) = J(\varepsilon, \phi) - \int_{\Omega} \phi^* M(\varepsilon, \phi) \mathrm{d}\mathbf{x} \tag{18}$$

where $\phi^* = (\mathbf{v}^*, p^*, T^*)^{\mathrm{T}}$ are the so-called adjoint variables, acting as Lagrange multipliers for the model equations. Optimization theory requires that all derivatives of L are zero in the optimum. The derivative with respect to the adjoint variables ϕ^* retrieves the state equations; the derivative with respect to the state variables ϕ results in the adjoint equations; the derivative with respect to the control variable ε results in the design equation.

We consider the derivation of the adjoint equations for a general objective functional:

$$J(\varepsilon, \phi) = \int_\Omega f(\varepsilon, \phi) \mathrm{d}\mathbf{x} + \int_{\partial\Omega} g(\phi) \mathrm{d}\mathbf{s} \tag{19}$$

The adjoint equations are retrieved from setting the derivative of L with respect to ϕ to zero for all variations ϕ'. We use subscript notation for the derivatives:

$$L_\phi(\varepsilon, \phi, \phi^*)\phi' = \int_\Omega f_\phi(\varepsilon, \phi)\phi' \mathrm{d}\mathbf{x} + \int_{\partial\Omega} g_\phi(\phi)\phi' \mathrm{d}\mathbf{s} - \int_\Omega \phi^* M_\phi(\varepsilon, \phi)\phi' \mathrm{d}\mathbf{x} = 0 \tag{20}$$

By partial integration, spatial derivatives are shifted from ϕ' to ϕ^* in the last term:

$$\int_\Omega \phi^* M_\phi(\varepsilon, \phi)\phi' \mathrm{d}\mathbf{x} = \int_\Omega \phi' M_\phi^*(\varepsilon, \phi)\phi^* \mathrm{d}\mathbf{x} + BT \tag{21}$$

where $M_\phi^*(\varepsilon, \phi)$ is the adjoint partial differential operator and BT gathers all boundary integrals appearing in the partial integration step. Requiring the domain integrals to vanish for all ϕ' results in the adjoint PDE system $M_\phi^*(\varepsilon, \phi)\phi^* = f_\phi$:

$$\nabla \cdot \mathbf{v}^* = f_p \tag{22}$$

$$-K_{\mathrm{c,m}}\rho\mathbf{v} \cdot \left(\nabla\mathbf{v}^* + (\nabla\mathbf{v}^*)^{\mathrm{T}}\right) = \nabla p^* + \nabla \cdot (\mu\nabla\mathbf{v}^*) - \alpha(\varepsilon)\mathbf{v}^* - K_{\mathrm{c,e}}\rho c T^* \nabla T + f_\mathbf{v} \tag{23}$$

$$-K_{\mathrm{c,e}}\rho c_p \mathbf{v} \cdot \nabla T^* = \nabla \cdot (k(\varepsilon)\nabla T^*) - k(\varepsilon)\frac{K_{\mathrm{d,e}}}{H^2} T^* + f_T \tag{24}$$

Requiring the boundary integrals to vanish for all ϕ' results in the adjoint boundary conditions:

$$\text{Inlet:} \quad p^* + K_{\mathrm{c,m}}\rho\mathbf{v} \cdot \mathbf{v}^* + K_{\mathrm{c,m}}\rho v_\mathrm{n} v_\mathrm{n}^* + \mu\frac{\partial v_\mathrm{n}}{\partial n} = g_{v_\mathrm{n}} \qquad v_\mathrm{t}^* = 0 \qquad T^* = 0 \tag{25}$$

$$\text{Outlet:} \quad p^* + K_{\mathrm{c,m}}\rho\mathbf{v} \cdot \mathbf{v}^* + K_{\mathrm{c,m}}\rho v_\mathrm{n} v_\mathrm{n}^* + \mu\frac{\partial v_\mathrm{n}}{\partial n} = g_{v_\mathrm{n}} \qquad v_\mathrm{t}^* = 0 \qquad K_{\mathrm{c,e}}\rho c_p v_\mathrm{n} + k\frac{\partial T^*}{\partial n} = g_T \tag{26}$$

$$\text{Walls:} \quad v_\mathrm{n}^* = 0 \qquad v_\mathrm{t}^* = 0 \qquad k\frac{\partial T^*}{\partial n} = g_T \tag{27}$$

The subscripts n and t are used to denote the normal and tangential velocity components. The coordinate n is the outward normal.

The gradient of the reduced cost functional is calculated using the derivative of the Lagrangian with respect to ε and the solutions ϕ and ϕ^* of the state and adjoint equations:

$$\hat{J}'(\varepsilon)\varepsilon' = L_\varepsilon(\varepsilon, \phi, \phi^*)\varepsilon' \tag{28}$$

$$= \int_\Omega \left(f_\varepsilon - \alpha_\varepsilon \mathbf{v} \cdot \mathbf{v}^* - k_\varepsilon \nabla T \cdot \nabla T^* + k_\varepsilon \frac{K_{\mathrm{d,e}}}{H^2} T^* (T_\mathrm{s} - T) \right) \varepsilon' \mathrm{d}\mathbf{x} \tag{29}$$

The adjoint method is applicable to the optimization problem (16) by identification of the general objective

function (19) with the total heat transfer. This yields:

$$f(\varepsilon, \phi) = k(\varepsilon)\frac{K_{\mathrm{d,e}}}{H^2}\left(T_{\mathrm{s}} - T\right) \qquad g(\phi) = 0 \tag{30}$$

4.2 Model implementation

The aforementioned state and adjoint equations are numerically solved in Matlab. The equations are discretized using the finite volume method on a structured, rectangular grid. The momentum equations are discretized on staggered grids. This is a standard CFD-approach to avoid checkerboard patterns in the pressure and velocity fields. The convective and diffusive fluxes are discretized with the hybrid scheme [27].

An iterative, implicit method to solve the coupled system of steady flow equations is used. Because the Reynolds number in microfluidics is typically low, solving the continuity and momentum equations together leads to a faster and more robust simulation method. This comes at the cost of a larger coefficient matrix. Another effect of the low Reynolds number is that no turbulence model is needed. After the flow field has been computed, the energy equation is solved in one linear system solve.

The additional convective term in the adjoint equations is discretized with the upwind scheme. The rest of the solution method is identical to the state equations, except for the order of energy and flow equations. The adjoint energy equation is solved first, because it is independent of $\mathbf{v}^*$ and p^*, whereas T^* appears in the adjoint flow equations. This reflects the nature of the adjoint method, which passes information in reverse order through the model, i.e. from output to input.

4.3 Optimization

The solution of the optimization problem (16) is found iteratively by the method of moving asymptotes (MMA). The MMA has been introduced by Svanberg [35] and is widely adopted for topology optimization problems. In each iteration, a convex, separable approximating subproblem is generated and solved. The solution of the subproblem is used for a new approximation. This procedure generates a sequence of approximate solutions that converges towards the solution of the original problem (16).

The approximating subproblem in the k-th iteration has the following form:

$$\begin{aligned} \min_{\varepsilon_i} \quad & r^k + \sum_i \left(\frac{p_i^k}{U_i^k - \varepsilon_i} + \frac{q_i^k}{\varepsilon_i - L_i^k} \right) \\ \text{subject to:} \quad & \\ & \underline{\varepsilon_i}^k \leq \varepsilon_i \leq \overline{\varepsilon_i}^k, \quad \forall i \end{aligned} \tag{31}$$

where ε_i is the discretized porosity. The parameters U_i^k, L_i^k, $\underline{\varepsilon_i}^k$ and $\overline{\varepsilon_i}^k$ are updated each iteration to control the robustness and speed of the convergence process. The parameters r^k, p_i^k and q_i^k are then determined to yield a first-order approximation of the original problem. This means that the value and gradient of the approximate objective function and the original objective function are the same. For each component of ε_i always one of p_i or q_i is zero, depending on the sign of the gradient.

The subproblem (31) is much easier to solve than the original problem, because of the convex, separable nature of the approximation to the objective function. Here, we use an implementation by Svanberg in Matlab. This algorithm controls the updating of U_i^k, L_i^k, $\underline{\varepsilon_i}^k$ and $\overline{\varepsilon_i}^k$ according to the principles in [35], and solves the subproblem with an interior-point method.

Table 1 Performance comparison of initial and optimized design.

	$\dot{Q}$ (W)	R_{hs} (K/W)	$\dot{m}$ (g/s)	$\dot{m}c_p$ (W/K)	hA (W/K)
Initial ($\varepsilon = 1$)	12.3	3.25	101	421	0.307
Free design at inlet	836 = 794.2$_{(\mathrm{outlet})}$ + 41.4$_{(\mathrm{inlet})}$	0.0478	9.25	38.7	30.0
Fixed design at inlet	794	0.0504	8.88	37.1	28.4

5. RESULTS

The method has been applied to a test case. The result of the optimization on a reference case is first shown and discussed. Next, a sensitivity analysis of key parameters is performed.

5.1 Reference case

Case description In the reference case, the size of the heat sink is $L \times W = 1\mathrm{cm} \times 1\mathrm{cm}$. The etch depth H is $500\mu\mathrm{m}$. The heat sink is made of silicon ($k_{\mathrm{s}} = 149\frac{\mathrm{W}}{\mathrm{m\cdot K}}$). The cooling fluid is pure water ($k_{\mathrm{f}} = 0.598\frac{\mathrm{W}}{\mathrm{m\cdot K}}$, $\mu = 1.004 \cdot 10^{-3}\mathrm{Pa\cdot s}$, $\rho = 998\frac{\mathrm{kg}}{\mathrm{m^3}}$, $c_p = 4180\frac{\mathrm{J}}{\mathrm{kg\cdot K}}$). The temperature difference between heat source and inlet of the heat sink is $\Delta T = 40\mathrm{K}$. The static pressure drop over the heat sink is $\Delta p = 10\mathrm{kPa}$.

The grid consists of $N_x = 200$ by $N_y = 200$ identical, rectangular cells. This is currently about the largest feasible grid for the present Matlab implementation. The design is initialized uniformly at $\varepsilon = 1$, which corresponds to a heat sink without fins, containing only fluid. The initial performance is found in Table 1. The value of the loss coefficient in the solid is taken at $\alpha_{\max} = \frac{K_{\mathrm{d,m}}}{H^2}$, which is 3 orders of magnitude larger than the value in the fluid $\alpha_{\min} = \mu\frac{K_{\mathrm{d,m}}}{H^2}$. The value of the interpolation parameter q is initially set at 0.01, and increased every optimization iteration until it reaches $q_{\mathrm{final}} = 1$ after 50 iterations. A similar approach is advised in [7] to avoid gettin stuck in suboptimal local minima. The algorithm is allowed to settle in 50 additional iterations. In all simulations, we observe no more significant changes to the design nor the total heat transfer.

During testing of the proposed methodology, convergence issues were detected in the forward model. These problems might be induced by local flow instabilities at too large Reynolds numbers in parts of the domain. In order to ensure a steady solution always exists, the present results are limited to Stokes flow. This means that we discard the convective momentum transport from the forward flow model, as well as its consequences in the adjoint flow model and boundary conditions.

Evaluation of results The corresponding optimized design is shown in Figure 2(a). In the greyscale images of the design, white corresponds to $\varepsilon = 1$ (fluid) and black corresponds to $\varepsilon = 0$ (solid). Looking at the energy balance, we observe that a significant fraction of the heat is removed by conduction at the inlet (Table 1: 'free design at inlet'). This is due to the inlet boundary condition, which imposes a fixed temperature. The optimizer takes advantage of this cold spot by placing a large amount of the high conductive solid material near the inlet (Fig. 2(a)). This is however not physically meaningful, as in reality a collector is attached to this side for flow distribution. To overcome this issue, we have further on fixed the design of the first cell near the inlet at $\varepsilon = 1$ (fluid only). The result of a new optimization run with this adjustment is shown in Figure 2(b).

The optimized design (Fig. 2(b)) consists of a number of macro-scale channels that branch into micro-scale channels, covering the whole surface of the heat sink. Each flow path from inlet to outlet passes through the micro-scale channels, which are sometimes even only one cell wide. Often, this connection occurs through what appears to be solid (black), which reflects that the solid is not perfectly impermeable in the model. The fraction of remaining grey cells is small as desired, which shows that $q_{\mathrm{final}} = 1$ is a good choice.

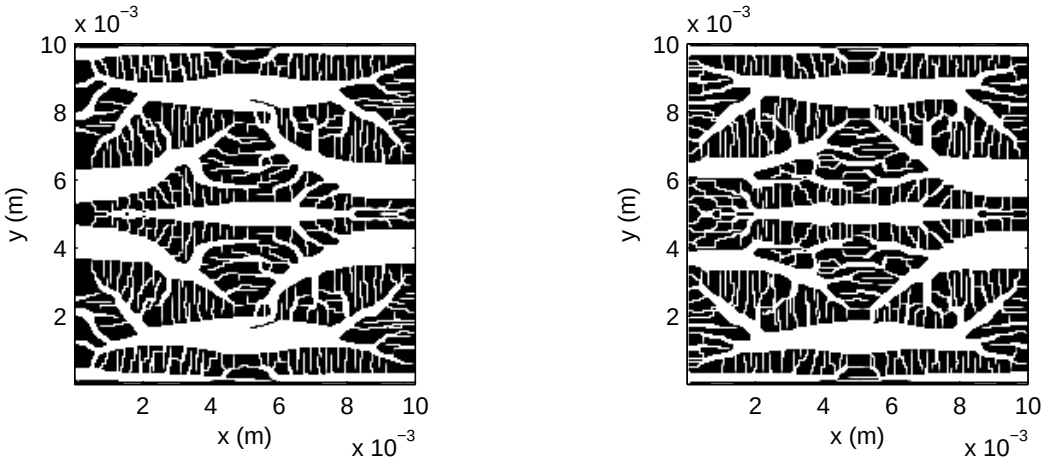

(a) Without design restriction: $\dot{Q} = 836\mathrm{W}$, of which $794\mathrm{W}$ by convection through the outlet and $41\mathrm{W}$ by artificial conduction through the inlet.

(b) With restricted design at the inlet (west boundary): $\dot{Q} = 794\mathrm{W}$.

Fig. 2 Optimized heat sink design (greyscale image of ε) in reference case.

The total heat transfer is $794\mathrm{W}$, which is a lot higher than the heat transfer in the initial design ($12.3\mathrm{W}$). This is expected as the initial design has no fins or other heat transfer enhancement structures. The influence of the fins in the optimized design is also clearly indicated by Figure 3(a). This shows the spatial distribution of the heat flux from the heat source, which goes mostly through the fins ($782\mathrm{W}$). Only a small fraction of the heat goes directly through the bottom plate to the fluid ($12\mathrm{W}$). Figure 3(a) shows that most of the heat transfer occurs near the inlet of the channel. This is explained by the larger temperature difference between the heat source and the flow. The latter increases in the streamwise direction due to the heat input, as shown in Figure 3(b).

The total mass flow rate through the optimized heat sink is $8.88\frac{\mathrm{g}}{\mathrm{s}}$. Since the static pressure drop is fixed, the mass flow rate is entirely determined by the flow resistance of the heat sink. This flow resistance is the result of two contributions: viscous stresses, both in-plane and out-of-plane, and Darcy stresses due to the porous-medium modeling. During the optimization, for each grid cell a balance is found between flow resistance and heat transfer. This interpretation is facilitated by considering the following integral heat sink model [24]:

$$\dot{Q} = \underbrace{\left(1 - e^{-\mathrm{NTU}}\right)}_{\text{effectiveness}} \dot{m} c_p \left(T_\mathrm{s} - T_\mathrm{i}\right) \tag{32}$$

$$\text{with } \mathrm{NTU} = \frac{hA}{\dot{m} c_p} \tag{33}$$

This shows that hA and $\dot{m}c_p$ are the determining parameters for the performance of the heat sink. hA is the integral heat transfer coefficient, as measured by the logarithmic mean temperature difference (LMTD) between heat source and flow. $\dot{m}c_p$ determines the temperature rise of the flow through the heat sink. The model shows that both parameters improve the total heat transfer $\dot{Q}$ when they increase. However, they are not independent, so a balance must be made. Table 1 shows that the performance of the initial design is dominated by the very low value of hA. In the optimized design, hA and $\dot{m}c_p$ are better balanced, having the same order of magnitude.

5.2 Sensitivity analysis

To assess the reliability of the optimized design, a sensitivity analysis of key parameters is performed. We look first at the operational parameters ΔT and Δp. Subsequently the numerical parameters, namely grid size, $\alpha_{\max}$

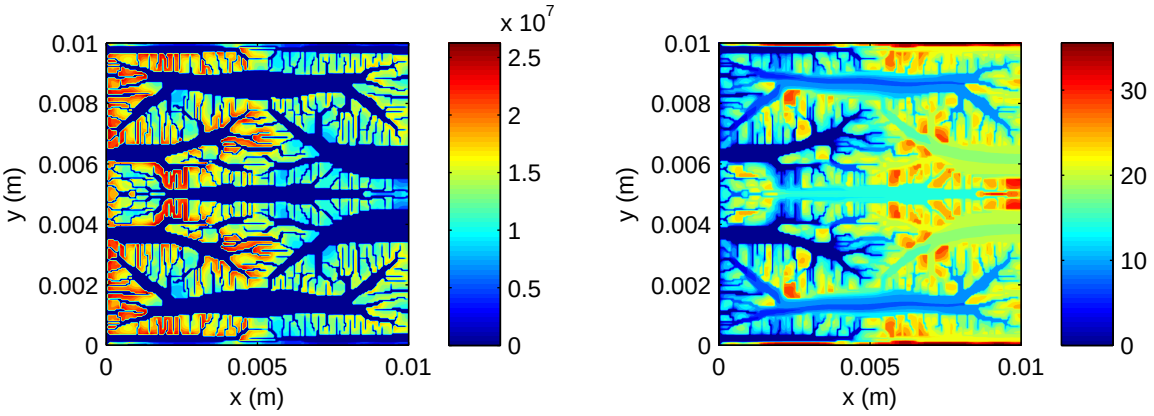

(a) Source heat flux $\dot{Q}''$ $\left(\frac{\mathrm{W}}{\mathrm{m}^2}\right)$ (b) Temperature T (K)

Fig. 3 Optimized source heat flux distribution and temperature field in reference case (with restricted design at inlet).

Table 2 Sensitivity analysis of key parameters. All variations are made with respect to the reference case with fixed (white) design at inlet.

	$\dot{Q}$ (W)	R_{hs} (K/W)	$\dot{m}$ (g/s)	$\dot{m}c_p$ (W/K)	hA (W/K)
Reference (fixed design at inlet)	**794**	**0.0504**	**8.88**	**37.1**	**28.4**
$\Delta T = 1\mathrm{K}$	19.5	0.0513	9.37	39.2	27.0
$\Delta p = 1\mathrm{kPa}$	197	0.203	1.40	5.84	10.8
$\Delta p = 100\mathrm{kPa}$	1668	0.0240	37.5	157	48.5
$N_x \times N_y = 100 \times 100$	800	0.0500	9.91	41.4	27.3
$\alpha_{\max} = 10K_{\mathrm{d,m}}/H^2$	454	0.0881	6.02	25.2	15.1
$q_{\mathrm{final}} = 0.1$	920	0.0435	10.8	45.3	32.1
$q_{\mathrm{final}} = 10$	791	0.0506	9.08	37.9	27.9

and q are discussed. All results of these cases are summarized in Table 2.

It is expected that the temperature difference ΔT between heat source and inlet has a linear influence on the total heat transfer, because the energy equation is linear. This means that the design and the thermal resistance would stay the same, independent of ΔT. However, the result for $\Delta T = 1\mathrm{K}$ shows a slight change in the thermal resistance (Table 2). This might indicate that there is more than one local solution of the optimization problem.

Table 2 shows that higher pressure drop results in a higher mass flow rate, which in turn increases the total heat transfer. This effect is sublinear, because the effect is only on $\dot{m}c_p$ and not on hA. The optimizer compensates this partly by shifting the balance between hA and $\dot{m}c_p$, so that both parameters increase when Δp increases. This balance shift is visible in the designs in Figure 4. The design with lower pressure drop has more and wider channels than the reference case. This means a lower flow resistance, attempting to compensate for the lower pressure drop. A price is payed by a lower hA-value. With the higher pressure drop, it's the other way around. However, since the finest scales are not resolved, the smallest channels are not visualized. They appear as flow through the black area.

The influence of the grid size is observed by looking at the result on a coarser grid with 100 by 100 cells. The total heat transfer is $800\mathrm{W}$, which is very close to the result on the 200x200 grid ($794\mathrm{W}$). However, when observing the contributions by $\dot{m}c_p$ and hA to this value in Table 2, we see that their relative change

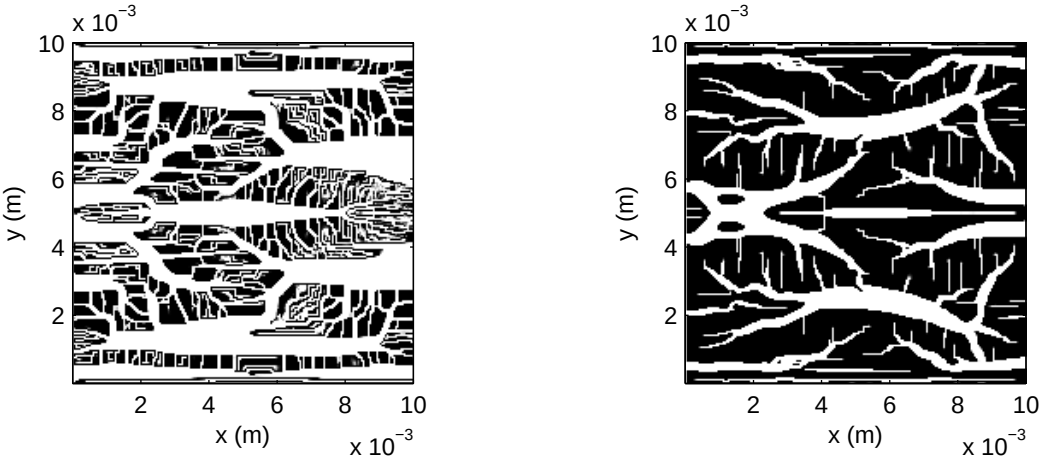

(a) $\Delta p = 1\text{kPa}$: $\dot{Q} = 197\text{W}$ (b) $\Delta p = 100\text{kPa}$: $\dot{Q} = 1668\text{W}$

Fig. 4 Optimized heat sink designs (greyscale image of ε), showing influence of static pressure drop.

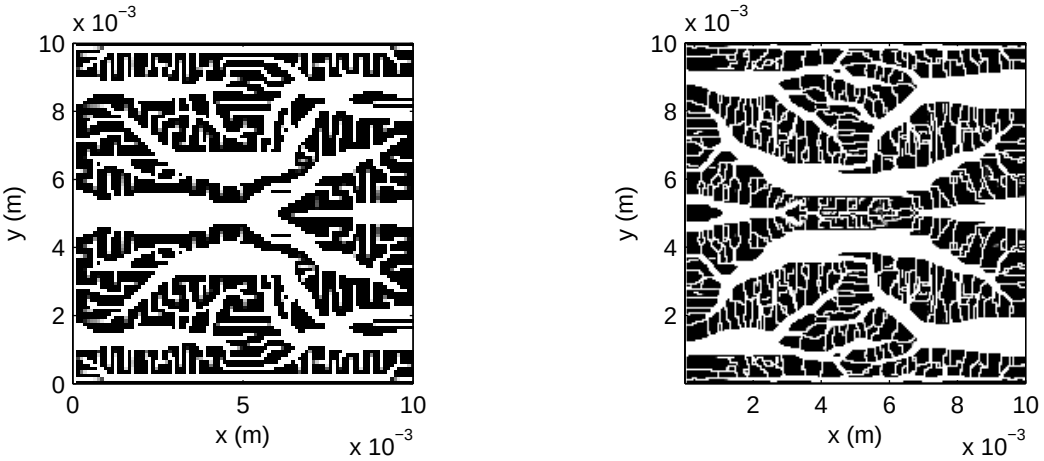

(a) 100 by 100 grid: $\dot{Q} = 800\text{W}$ (b) $\alpha_{\max} = 10\frac{K_{\text{d,m}}}{H^2}$: $\dot{Q} = 454\text{W}$

Fig. 5 Optimized heat sink design (greyscale image of ε).

is larger. This is a consequence of the overly coarse discretization of the finest channels. Spatial gradiënts in velocity and temperature are therefore underestimated. This is accompagnied by an overestimation of $\dot{m}c_p$ and an underestimation of hA. Their cumulative effect compensates each other partly, which explains why the value of $\dot{Q}$ is less affected. The corresponding designs, see Figures 2(b) and 5(a), are qualitatively similar. However, a grid independent solution is not yet obtained. Model accuracy and manufacturability of the design are therefore a concern. A method for controlling the size of the smallest structures and channels in the heat sink is needed to further improve the design.

The influence of the parameter $\alpha_{\max}$, the 'cost' of solid material in the sense of flow resistance, is shown in Figure 5(b). Here, the optimization has been repeated with a value 10 times larger: $\alpha_{\max} = 10\frac{K_{\text{d,m}}}{H^2}$. As expected, it is observed that the connectivity between inlet and outlet is increased. Indeed, less flow has to go through the black area, because this has become less permeable. The effect on the total heat transfer, which is reduced to 454W, and consequently on $\dot{m}c_p$ and hA values is remarkable. This means that the estimation of the heat transfer in the reference case is still depending on the permeability of the solid. This would mean that a permeable silicon layer would be advantageous, at least when no penalty has to be paid with respect to the thermal conductivity. As the latter requirement is hard to fulfill, the case with higher $\alpha_{\max}$ value seems to be

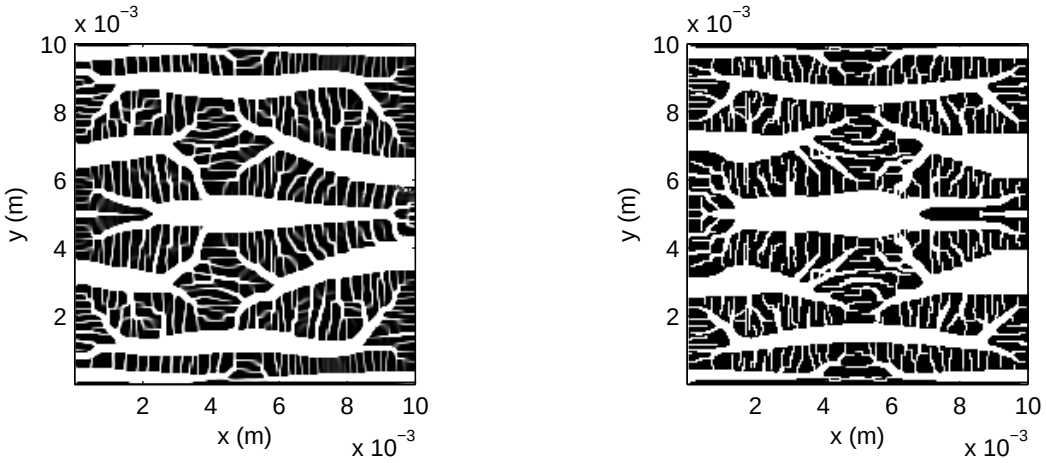

(a) $q_{\mathrm{final}} = 0.1$: $\dot{Q} = 920\mathrm{W}$ (b) $q_{\mathrm{final}} = 10$: $\dot{Q} = 791\mathrm{W}$

Fig. 6 Optimized heat sink design (greyscale image of ε, showing influence q_{final}.

more realistic.

Finally, the last parameter to investigate is q_{final}, which controls the value of α for intermediate values of ε. The larger q_{final}, the higher α in the grey areas. When q_{final} is lowered to 0.1, we observe a smoother design, containing a bit more grey areas. The heat transfer is significantly larger than in the reference case, a result of the higher mass flow rate. At the larger value of $q_{\mathrm{final}} = 10$, all grey has practically vanished. This is favorable for the post-processing of the result, but contains a risk of getting stuck in a local optimum. The total heat transfer is in this case similar to the reference case, indicating that $q_{\mathrm{final}} = 1$ was a good choice.

6. DISCUSSION

The layout of the optimized designs that emerge as results of our method, is best described as a tree-like network of channels. Large channels branch into smaller channels, distributing the flow over the heat sink. In these small-scale channels, a large part of the total heat transfer enters the fluid. Eventually, the flow is again recollected in the larger channels and flows through the outlet. This cooling concept, as obtained by automated topology optimization, reminds us of cooling solutions proposed by Bejan & Errera (e.g. in [4]).

However, in contrast, their work is based on the constructal principle that the core task of a heat exchanger is performed at the smallest scale. These smallest channels are then optimized first, followed by assembling the optimal heat exchanging element in larger and larger constructions. These constructions are designed for optimal flow distribution towards the heat exchanging element.

We would also like to mention the work by Pence [28], whose work focussed on the design of radial heat sinks. In a radial heat sink, the inlet is in the middle and the outlet is distributed over the circumference of the heat sink. In [28], fractal-like flow networks were proposed to connect inlet and outlet. This is very similar to the concept in [4], but without recollecting the flow, which is not necessary because the outlet is much larger than the inlet.

Thus, it can be concluded that topology optimization for thermal design of heat sinks leads to tree-like network designs and as such confirms, at least partially, the design concepts proposed earlier. Further, it is clear that the proposed methodology has its own assets. First, the present results have been obtained without a priori assumptions about the layout. Secondly, the method is more flexible than the parametric studies used. In these earlier studies, representative elements are optimized without guaranteeing the optimal design of the whole heat sink. In this context, it should be noted that the present results do not indicate that repetitive structures

are favorable for the global optimal design. Thirdly, the method can be extended to incorporate other operating conditions such as a non-uniform heat source temperature, fixed heat source flux distribution or different inlet/outlet configurations. Finally, the present methodology can be extended to incorporate minimal channel or fin size constraints, in order to further refine the fully automated design methodology.

7. SUMMARY & CONCLUSIONS

In this paper, we have applied topology optimization to the cooling of a constant temperature heat source. This method optimizes the locations where fins and channels should form. To this end, a thermo-hydraulic model is developed to simulate the performance of the heat sink. This model consists of a two-dimensional PDE system, which incorporates essential interactions with the top and bottom walls. The design is represented by the porosity of the medium. The mapping of local porosity to the relevant parameters α and k is therefore an important aspect of the heat sink model. Based on the formulation of the optimization problem, the adjoint equations have been derived. The solution of these equations is used for efficient computation of the gradient of the objective functional. The discretization and solution procedure for the state and adjoint equations, as well as the optimization problem are discussed.

The method is tested on a case study involving the Stokes flow model, i.e. without inertial forces. The results in this case display a branching flow network, where the flow is distributed by large channels towards small-scale channels and then recollected again. The spatial distribution of heat transfer is discussed. The overall performance of the heat sink is interpreted using a simple heat exchanger model. This shows how the optimized design balances heat transfer and flow resistance. A sensitivity analysis of key parameters is performed.

It can be concluded that topology optimization is a suitable method for heat sink design. However, care needs to be taken to use high enough values of $\alpha_{\max}$, as to avoid artificial flows through solid material. The topology optimization method leads to branching, tree-like flow network designs. Further work is needed to incorporate technological constraints with respect to minimal feature size.

ACKNOWLEDGMENTS

The authors are grateful for the financial support from the Agency for Innovation by Science and Technology in Flanderss (IWT). Also the help and advice from KU Leuven colleagues is much appreciated, both from the Division of Applied Mechanics (TME) as well as from the Center of Excellence: Optimization in Engineering (OPTEC).

REFERENCES

[1] Andreasen, C. S., Gersborg, A. R., and Sigmund, O., "Topology optimization of microfluidic mixers," *International Journal for Numerical Methods in Fluids*, 61, pp. 498–513, (2009).

[2] Barrau, J., Rosell, J., Ibañez, M., and Tadrist, L., "High heat flux heat sink with adaptable distribution of the heat extraction capacity," *Proceedings of the 16th International Workshop on Thermal Investigations of ICs and Systems*, Barcelona, Spain, pp. 49–52, 6–8 October 2010.

[3] Bau, H. H., "Optimization of conduits' shape in micro heat exchangers," *International Journal of Heat and Mass Transfer*, 41, pp. 2717–2723, (1998).

[4] Bejan, A. and Errera, M. R., "Convective trees of fluid channels for volumetric cooling," *International Journal of Heat and Mass Transfer*, 43, pp. 3105–3118, (2000).

[5] Bejan, A. and Morega, A. M., "Optimal arrays of pin fins and plate fins in laminar forced convection," *ASME Journal of Heat Transfer*, 115, pp. 75–81, February 1993.

[6] Bendsøe, M. P. and Sigmund, O., *Topology optimization: Theory, methods and applications*, 2nd Edition, Springer Verlag, Berlin, (2004).

[7] Borrvall, T. and Petersson, J., "Topology optimization of fluids in Stokes flow," *International journal for numerical methods in fluids*, 41, pp. 77–107, (2003).

[8] Chen, C.-W., Lee, J.-J., and Kou, H.-S., "Optimum thermal design of microchannel heat sinks by the simulated annealing method," *International Communications in Heat and Mass Transfer*, 35, pp. 980–984, (2008).

[9] Colgan, E. G., Furman, B., Gaynes, M., Graham, W. S., LaBianca, N., Magerlein, J. H., Polastre, R. J., Rothwell, M. B., J., B. R., Choudhary, R., Marston, K. C., Toy, H., Wakil, J., Zitz, J. A., and Schmidt, R. R., "A practical implementation of silicon microchannel coolers for high power chips," *IEEE transactions on components and packaging technologies*, 30(2), pp. 218–225, June 2007.

[10] Copeland, D., Behnia, M., and Nakayama, W., "Manifold microchannel heat sinks: isothermal analysis," *IEEE transactions on components, packaging, and manufacturing technology – part A*, 20(2), pp. 96–102, (1997).

[11] Dede, E. M., "Multiphysics optimization, synthesis, and application of jet impingement target surfaces," *Proceedings of 12th Thermal and Thermomechanical Phenomena in Electronics Systems (ITherm)*, pp. 1–7, (2010).

[12] Fisher, T. S. and Torrance, K. E., "Constrained optimal duct shapes for conjugate laminar forced convection," *International Journal of Heat and Mass Transfer*, 43, pp. 113–126, (2000).

[13] Harpole, G. M. and Eninger, J. E., "Micro-channel heat exchanger optimization," *7th IEEE Semi-Therm Symposium*, pp. 59–63, (1991).

[14] Husain, A. and Kim, K.-Y., "Optimization of a microchannel heat sink with temperature dependent fluid properties," *Applied Thermal Engineering*, 28, pp. 1101–1107, (2008).

[15] Husain, A. and Kim, K.-Y., "Shape optimization of micro-channel heat sink for micro-electronic cooling," *IEEE Transactions on Components and Packaging Technologies*, 31(2), pp. 322–330, June 2008.

[16] Kandlikar, S. G. and Upadhye, H. R., "Extending the heat flux limit with enhanced microchannels in direct single phase cooling of computer chips," *IEEE SEMI-THERM Symposium*, (2005).

[17] Kim, S. J., "Methods for thermal optimization of microchannel heat sinks," *Heat Transfer Engineering*, 25(1), pp. 37–49, (2004).

[18] Knight, R. W., Goodling, J. S., and Hall, D. J., "Optimal thermal design of forced convection heat sinks-analytical," *ASME Journal of Electronic Packaging*, 113, pp. 313–321, (1991).

[19] Knight, R. W., Hall, D. J., Goodling, J. S., and Jaeger, R. C., "Heat sink optimization with application to microchannels," *IEEE Transactions on Components, Hybrids, and Manufacturing Technology*, 15(5), pp. 832–842, October 1992.

[20] Kou, H.-S., Lee, J.-J., and Chen, C.-W., "Optimum thermal performance of microchannel heat sink by adjusting channel width and height," *International Communications in Heat and Mass Transfer*, 35, pp. 577–582, (2008).

[21] Li, H.-Y., Chiang, M.-H., and Chen, K.-Y., "Performance analysis of pin-fin heat sinks with confined impingement cooling," *IEEE transactions on components and packaging technologies*, 30(3), pp. 383–389, September 2007.

[22] Li, J. and Peterson, G. P., "Geometric optimization of a micro heat sink with liquid flow," *IEEE Transactions on Components and Packaging Technologies*, 29(1), pp. 145–154, March 2006.

[23] Li, J. and Peterson, G. P., "3-dimensional numerical optimization of silicon-based high performance parallel microchannel heat sink with liquid flow," *International Journal of Heat and Mass Transfer*, 50, pp. 2895–2904, (2007).

[24] Lienhard IV, J. H. and Lienhard V, J. H., *A heat transfer textbook*, 3rd Edition, Phlogiston Press, (2008).

[25] Liu, D. and Garimella, S. V., "Analysis and optimization of the thermal performance of microchannel heat sinks," *International Journal for Numerical Methods in Heat & Fluid Flow*, 15(1), pp. 7–26, (2005).

[26] Okkels, F., Olesen, L. H., and Bruus, H., "Applications of topology optimization in the design of micro- and nanofluidic systems," *NSTI-Nanotech*, (2005).

[27] Patankar, S. V., *Numerical Heat Transfer and Fluid Flow*, Series in Computational Methods in Mechanics and Thermal Sciences, Hemisphere Publishing Corporation, (1980).

[28] Pence, D., "The simplicity of fractal-like flow networks for effective heat and mass transport," *Experimental Thermal and Fluids Science*, 34, pp. 474–486, (2010).

[29] Ryu, J. H., Choi, D. H., and Kim, S. J., "Numerical optimization of the thermal performance of a microchannel heat sink," *International Journal of Heat and Mass Transfer*, 45, pp. 2823–2827, (2002).

[30] Ryu, J. H., Choi, D. H., and Kim, S. J., "Three-dimensional numerical optimization of a manifold microchannel

heat sink," *International Journal of Heat and Mass Transfer*, 46, pp. 1553–1562, (2003).

[31] Shaeri, M. and Yaghoubi, M., "Thermal enhancement from heat sinks by using perforated fins," *Energy Conversion and Management*, 50(5), pp. 1264–1270, May 2009.

[32] Shah, R. K. and London, A. L., *Laminar flow forced convection in ducts, a source book for compact heat exchanger analytical data*, Advances in Heat Transfer, Supplement I, Academic Press, New York, (1978).

[33] Stevens, T., Rogiers, F., and Baelmans, M., "Optimisation of micro-channel heat sink geometry," *13th International Heat Transfer Conference*, Sidney, Australia, August 2006.

[34] Sung, M. K. and Mudawar, I., "Single-phase hybrid micro-channel/micro-jet impingement cooling," *International Journal of Heat heat and Mass Transfer*, 51, pp. 4342–4352, (2008).

[35] Svanberg, K., "The method of moving asymptotes - a new method for structural optimization," *International Journal for Numerical Methods in Engineering*, 24, pp. 359–373, (1987).

[36] Tuckerman, D. B. and Pease, R. F. W., "High-performance heat sinking for VLSI," *IEEE Electron Device Letters*, 2(5), pp. 126–129, May 1981.

[37] Wechsatol, W., Lorente, S., and Bejan, A., "Dendritic heat convection on a disc," *International Journal of Heat and Mass Transfer*, 46, pp. 4381–4391, (2003).

[38] Wei, X. and Joshi, Y., "Optimization study of stacked micro-channel heat sinks for micro-elctronic cooling," *IEEE transactions on components and packaging technologies*, 26(1), pp. 55–61, March 2003.

[39] Wei, X. and Joshi, Y., "Stacked microchannel heat sinks for liquid cooling of microelectronic components," *ASME Journal of Electronic Packaging*, 126, pp. 60–66, March 2004.

[40] Weisberg, A., Bau, H. H., and Zemel, J. N., "Analysis of microchannels for integrated cooling," *International Journal of Heat heat and Mass Transfer*, 35(10), pp. 2465–2474, (1992).

[41] Yin, X. and Bau, H. H., "Micro heat exchangers consisting of pin arrays," *ASME Journal of Electronic Packaging*, 119, pp. 51–57, March 1997.

[42] Yin, X. and Bau, H. H., "Uniform channel micro heat exchangers," *ASME Journal of Electronic Packaging*, 119, pp. 89–94, June 1997.

[43] Zdravkovich, M., *Flow around circular cylinders*, Vol. 1, Oxford Science Publication, (1997).